KSME

Springer

Journal of Mechanical Science and Technology 35 (7) 2021

Original Article
DOI 10.1007/s12206-021-0613-1

Keywords:
· Hot press sintering
· Al-B_4C coating
· Wear
· MMCs

Correspondence to:
Cetin Ozay
cozay@firat.edu.tr

Citation:
Ozay, C., Ballikaya, H., Dagdelen, F., Karlidag, O. E. (2021). Microstructural and wear properties of the Al-B_4C composite coating produced by hot-press sintering on AA-2024 alloy. Journal of Mechanical Science and Technology 35 (7) (2021) 2895~2901.
http://doi.org/10.1007/s12206-021-0613-1

Received January 29th, 2021
Revised March 5th, 2021
Accepted March 30th, 2021

† Recommended by Editor Chongdu Cho

Microstructural and wear properties of the Al-B_4C composite coating produced by hot-press sintering on AA-2024 alloy

C. Ozay[1], H. Ballikaya[2], F. Dagdelen[3] and O. E. Karlidag[1]

[1]Faculty of Technology, Mechanical Engineering Department, Firat University, 23119 Elazig, Turkey, [2]Department of Machine and Metal Technologies, Malatya Organized Industrial Zone Vocational High School, Inonu University, 44100 Malatya, Turkey, [3] Physics Engineering Department, Faculty of Science, Firat University, 23119 Elazig, Turkey

Abstract In this study, the surface of an AA-2024 alloy was covered with reinforced composite coating using hotpress sintering method. Al and B_4C powders were synthesized through mechanical alloying technique and coated on the AA-2024 substrate at different rates. The microstructure of the intermediate transition region formed between the substrate (AA-2024 Al alloy) and the coating layer (Al/B_4C MMCs), the microstructure of the Al/B_4C metal matrix composites (MMCs) coating, the microhardness, and the adhesive wear resistance of the Al/B_4C MMCs coating layer were investigated. It was observed that B_4C powders homogeneously dispersed in the microstructure of the Al/B_4C MMCs coating layer, moreover, the Al matrix and B_4C reinforcement particles were bonded without a gap. It was also determined that an interface bonding occurred between Al/B_4C MMCs coating layer and the AA-2024 substrate. Accordingly, it was determined that with the increase of B_4C reinforcement particle ratio, the hardness of the coating layer, and the wear resistance increased.

1. Introduction

Vehicles and systems produced in recent years need to be light and high-strength to use energy efficiently. In this respect, some features such as high strength/ weight ratio, easy forming and processing, low density, good thermal and electrical conductivity, high corrosion resistance, high-toughness, and endurance in Al-based alloys must have be improved. Among aluminum alloys, AA-2024 alloy, which main alloying element is copper, comes into prominence because of its characteristics such as formability, age hardening, elastic modulus, mechanical strength [1].

Many coating techniques such as arc weld [2, 3], micro-arc oxidation [4, 5], plasma spraying [6, 7], sol-gel [8, 9], reactive magnetron sputtering [10, 11], laser [12, 13], and rarely with vacuum hotpress sintering [14-16], used by different researchers to improve material surface. Coating of a metal surface with MMCs enables different characteristics to assemble on the coating layer. Coating of Al alloys also takes an important place [8, 17-19]. Coating processes provide features, e.g., mechanical, thermal, and electrical conductivity, high damping capability, resistance to oxidation, low density, and good wear resistance [20]. In MMCs materials, due to very great hardness, wear and impact resistance, good chemical stability, use of reinforcement particles such as B_4C [21-26], SiC [27-29], $A_{l2}O_3$ [16, 30], TiC [31-33] has increased. Especially, particle-reinforced composites with aluminum metal matrix composites (AMMCs) are preferred in space, aviation, automotive, and many other sectors because of their high strength/weight ratio, good mechanical and non-magnetic features (paramagnetic substances) [34, 35]. Besides, AMMCs are preferred because they help design lighter products and significantly increase fuel efficiency to reduce material weight by more than 50 % compared to low-carbon steels [36].

In recent years, most coating and protection techniques have been used to refine the surface

Table 1. The chemical compound of AA-2024 aluminum alloy.

Fe	Si	Cu	Cr	Mn
0.5	0.5	3.8-4.9	0.1	0.3-0.9
Mg	Zn	Ti	Al	-
1.2-1.8	0.25	0.15	Balanced	

Fig. 1. Unit for coating AA-2024 substrate with Al-B_4C composite.

of AA-2024 alloy, which is widely used in space, aviation, and automotive technologies. However, there is no study that investigated the use of the hot press sintering method in the coating of AA-2024 substrate materials. In this study, the AA-2024 alloy surface was coated with Al-B_4C MMCs, using the hot press sintering method. Surface morphology of AMMCs coating layer and interface microstructure formed on the substrate, the microhardness of coating layer, and wear resistance have been thoroughly investigated.

2. Experimental procedure

Fig. 1 shows the experimental setup designed for coating the AA-2024 substrate with Al-B_4C. In this study, firstly, the powders were mixed, and then the substrate used in experimental studies was prepared in Ø12x5 mm by measure. Table 1 lists the chemical compositions and their corresponding ratio used in the AA-2024 alloy substrate. The substrate was mechanically cleaned to remove the oxide layer and residual material from the surface, then washed with alcohol and dried.

For the coating layer, Al powder with size of 44 µm and purity of 99.5 % was used, also B_4C powder used in this study had 99 % purity with average particle size of 10 µm. The volumetric powder ratio used on the coating layer and production parameters can be seen in Table 2. To ensure the homogenization of the coating powders, balls with a diameter of 10 and 5 mm and with ratio of 1:1, and ball powder with ratio of 15:1 were mixed in 3-axis turbula mixer 3 at 350 rpm for about 25 minutes.

To form the AMMCs coating layer, firstly the die was prepared, and a HSS lamella with dimension of Ø12X5 mm was placed at the bottom. Then, it was placed after the cleaned coating surface of AA-2024 alloy substrate. Al/B_4C powder

Table 2. Production parameters of AA-2024 substrate coating with Al-B4C.

Production parameters	Samples			
	S1	S2	S3	S4
B_4C particle reinforcment ratio % vol	0	2.5	5	8
Weighting pressure MPa	110			
Sintering temperature °C	575			
Shielding gas	99 % argon gas			

mixture was poured over an AA-2024 alloy pad in the die.

Later, an upper piston lamella made of HSS material was put on Al/B_4C powder mixture to use as upper-pressure piston. The matrix was heated up to 575 °C in the Core Mf 129 oven operating in an argon gas atmosphere and kept at this temperature for 20 minutes. Then, the sample at 575 °C was pressed under a pressure of 110 MPa on a specially designed (in argon gas environment) press bench and was kept under pressure for 5 minutes to cool down in that environment.

For XRD examinations, the coating surface of Al/B_4C MMCs of the samples was mechanically cleaned, washed with alcohol, and dried. XRD was taken with the help of Rigaku Miniflex 600 diffractometer, which scanned for the range of 20-90° and with 0.005° step range, also CuKα radiation (λ = 0.15406 Å) was utilized. Samples, prepared for microstructure examinations, (2 ml HF + 3 ml HCl + 5 ml HNO_3 + 190 ml water) were etched with keller solution for about 30 seconds. To analyze the distribution of microstructure and rigid phases in the structure, Nikon Eclipse MA200 brand optical microscope (OM) with Clemex Software and Tescan Mira3 equipment for SEM-EDS were used. Microhardness measurements were taken in Emcotest Durascan 20 device by applying a load of 50 g for 10 seconds. Microhardness measurements were evaluated by taking the arithmetic mean of the values taken from 10 different points in the cross-section of the samples. The coating surface was cleaned and dried for wear samples. Linear reciprocating wear tests were carried out under ASTM G133 standards in CSM/Anton Paar Instrument Tribometer device using a ball-on-disc mechanism. These tests were carried out under 1 N force, 250 m sliding distance, and ASTM A276 against material conditions.

3. Results and discussion

3.1 XRD analysis

Fig. 2 reveals the XRD pattern obtained for the S1 and S4 samples. The XRD graphics were taken from the surface of the MMCs coating layer, where the AA-2024 alloy is coated with Al- B_4C powders. The XRD provides sharp peaks indicated Al and B_4C phases [23, 37-39]. The Al phase peaks are the prominent peaks compared with those of B_4C. The reason could be the lower volume friction of the B_4C phase in the structure [40]. The peaks of the B_4C phase are given in Fig. 2(c). The Al main matrix peaks forming the coating layer can be seen at 38, 45, 65, and 78°, and the reflection planes are

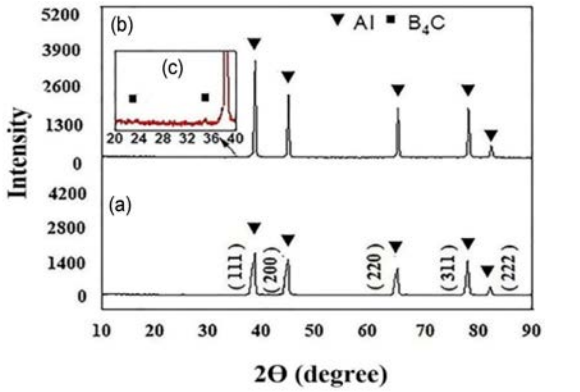

Fig. 2. The XRD pattern of samples: (a) S1; (b) S4 sample; (c) the inset of the XRD pattern magnified some selected region of the S4 sample.

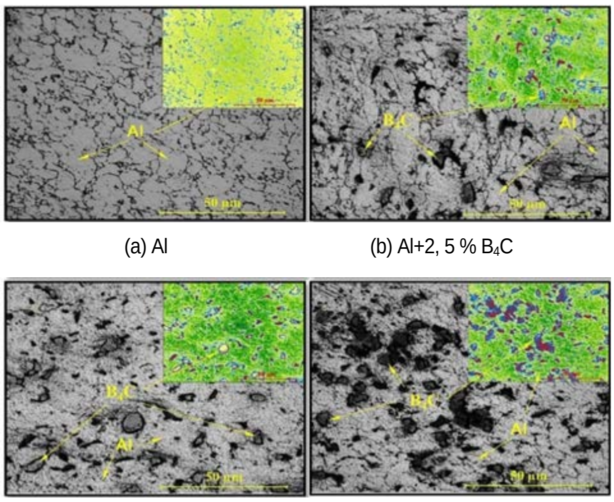

(a) Al (b) Al+2, 5 % B_4C

(c) Al+5 % (d) Al+8 % B_4C

Fig. 3. OM images of produced AMMCs coating layer.

(111), (200), (220), (311), and (222), respectively [23]. The peaks of B_4C reinforcement particles were determined at 23.35°.

3.2 Micro-structural analysis

Fig. 3 shows the OM images of the coated layer for both samples. It can be seen that Al and B_4C powders, which formed MMCs coating layer are well mixed up and B_4C particles have been broken down through mechanical mixing process. In Fig. 3(a), reveals the OM image of AA-2024 coated with Al powder. Besides, Figs. 3(b)-(d) show the OM images of Al-B_4C samples with different compositions that were hot-pressed on the substrate. The B_4C particles in S2, S3, and S4 samples are homogeneously dispersed and there is no coagulation in the structure. As the reinforcement material ratio on the coating layer increased, B_4C particles were clearly seen in the OM images.

In Fig. 4, SEM images of coating layer interfaces taken from cross-section of the samples are given. In Fig. 4(a), a certain area between AA-2024 substrate and a coating is formed that indicates a metallurgical bond with a good dampening, moreover, there are no pores and cracks. It was determined that there is porous space in this area and the porosity decreases as it approaches the coating layer. The growth of pores in the diffusion region can be explained in terms of the Kirkendall effect. This is because Al tends to diffuse from the AA-2024 substrate surface towards the coating layer during the sintering process, moreover, when elements transit from the surface, i.e., from alloy to the coating layer, they leave pores on the aluminum powder coating due to the difference in diffusion velocity. Due to the difference in mobility of alloying elements, it is expected that they leave pores behind during the cooling process [37-39]. In Figs. 4(b)-(d), it is seen that B_4C particles homogeneously disperse in the Al matrix. There isn't any coagulation, while a diffusion region between substrate and coating layer can be seen. EDS analyses taken from these transition regions reveal a diffusion from substrate towards coating layer. At the X2000 magnified photo taken from the coating layer of S2 and S3 samples, it is found that the Al matrix surrounds B_4C reinforcement particles and there is no gap (Figs. 4(b) and (c)).

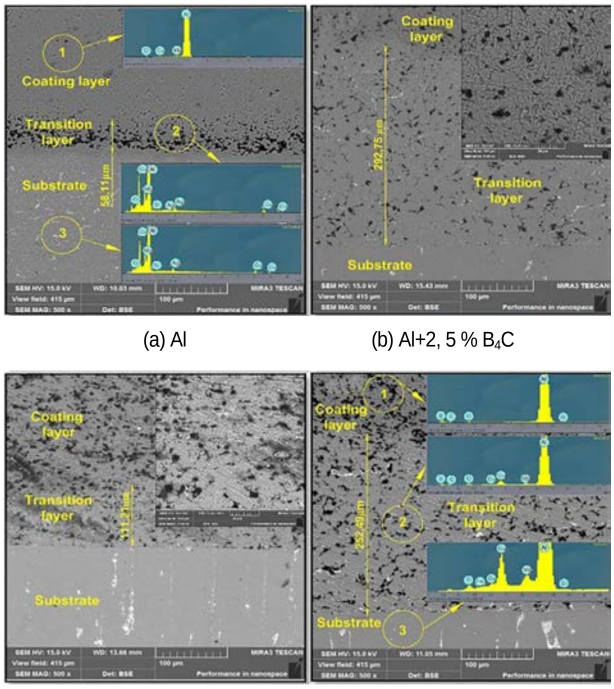

(a) Al (b) Al+2, 5 % B_4C

(c) Al+5 % B_4C (d) Al+8 % B_4C

Fig. 4. SEM images and EDS analyses of interface microstructure of samples.

3.3 Micro-hardness and wear analysis

Hardness is a significant mechanical property to investigate the protective layer on the surface of materials. Because the hardness of the coating layer affects the wear resistance of the material [3], measurements of HV microhardness and weight loss from wear have been taken from the coating layer of the

Table 3. Microhardness and weight loss as a function of B_4C volume fraction.

Sample	Weight loss (mg)	Microhardness (HV)
S1	10	38,8
S2	13	42,6
S3	0.7	57,6
S4	0.6	51,9

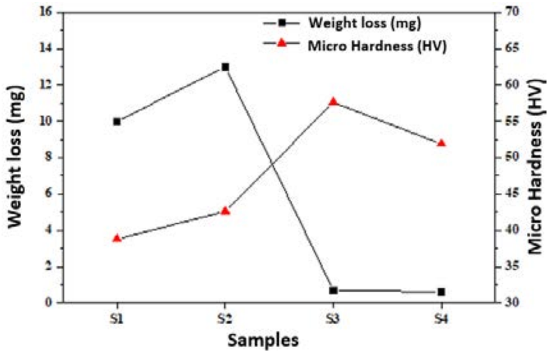

Fig. 5. Microhardness and weight loss in relation to B_4C volume ratio of samples.

samples. The results acquired are given in Table 3 and Fig. 5. When these results are examined, it is found that the hardness value increases with the increase of B_4C ratio in the coating layer, while the weight loss decreases [40, 41].

By analyzing the results given in Table 3, Figs. 5 and 6, it is stated that the microhardness of the S1 sample coated with pure Al powder is low and it has a high weight loss. The increase of the B_4C ratio, which is known as a hard particle, enhances wear resistance and decreases weight loss due to the decline in contact area on the wear surface [24]. Although the B_4C ratio in S2 is 2.5 % and microhardness is higher than S1, the sample lost more weight due to the delamination wear mechanism caused by deposits during wear process. As can be seen from the OM images in Fig. 3(b), high weight loss has occurred in S2 due to the stress induced around B_4C particles, therefore it indicates that Al matrix and B_4C reinforcement particles well mixed and thus breaking off in a layer during wear. When loading is applied to composite materials produced by powder metallurgy, stress is induced around the hard reinforced particles. In Fig. 6(b), the crack observed just below the worn surface shows that high plastic stress emerges in the matrix at high temperatures and matrix is in direct contact with the material. Strain gradients that created beneath the contact surface cause subsurface crack propagation and the wear progresses through subsurface delamination [42]. In general, the microhardness increases with the rise of the B_4C ratio in the coating layer [43]. However, the hardness of the S4 is slightly less than the hardness of the S3. Also, the reducing weight loss of S3 and S4 is due to increasing microhardness (Figs. 6(c) and (d)). Besides, some researchers [44-47] have

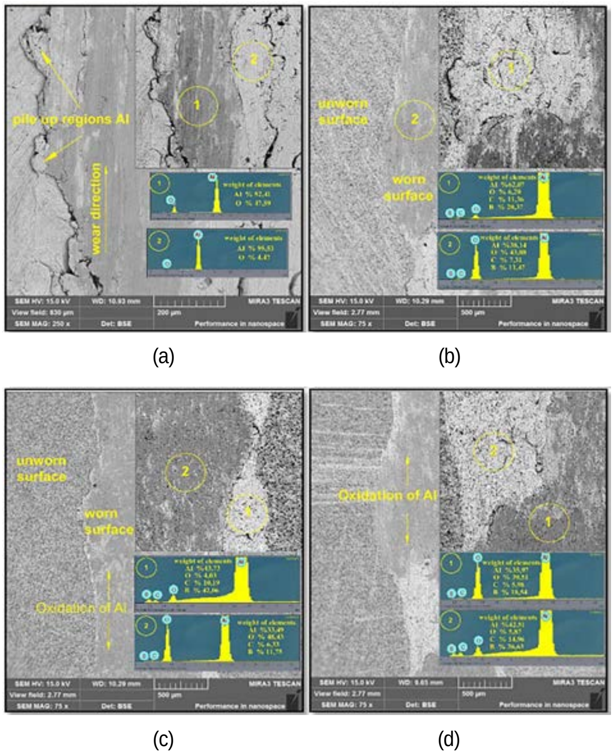

Fig. 6. SEM images and EDS analyses of interface microstructure of the samples.

suggested that the formation of aluminum oxide and boron oxide during wear diminishes the friction coefficient, and thus reduces wear loss. The EDS analysis taken from region #1 of worn samples, displays that oxygen level is low while it is detected with a higher ratio in region #2. Also in region #2 a layer formed that resisted to wear.

Fig. 7 shows the friction coefficient of samples coated with Al/B_4C MMCs, depending on sliding distance during adhesive wear. The friction coefficient is important evidence for the understanding of wear and friction performance of the materials [48]. From Fig. 7 it can be seen that friction coefficient curves in adhesive wear increase rapidly until they reach the highest value and then gradually decrease and finally it reaches a plateau. The friction coefficient curves of S1 increase to 1.20 as the highest value, then reached a constant value around 0.38, and finally gradually declined, depending on the sliding distance.

The friction coefficient showed a high fluctuation in S2 at the first stage, depending on the sliding distance. It reached the highest value at 0.96 and the stable value at 0.5. The reason for the high fluctuation in S2 is due to the local surface fracture and the accumulation of debris formed during wearing. On the other hand, its steady-state shows that the fractures are moving away from the surface [49]. S3 has shown a more stable fluctuation in friction coefficient than other examples. Also, it is seen that it changes around 0.72 and 0.54. In S4, while there is a fluctuation in the first case, it becomes stable in the course of

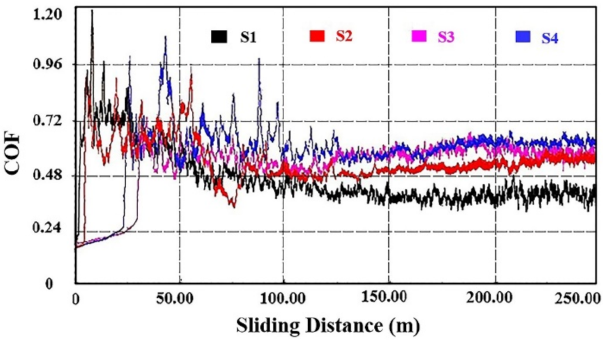

Fig. 7. The friction coefficient of produced AMMCs coating layers.

time, and the friction coefficient changes between 1.1 and 0.6. The fluctuation of friction coefficient in the first 100 m of wear distance is related to the accumulation of debris on the surface and their removal from the surface. While friction coefficient increases with the accumulation of debris, it decreases with their removal from the surface. Low fluctuation in coefficient is a sign of oxidation wear or small deposits [50].

4. Conclusions

In this study, Al/B_4C AMMCs were coated through the AA-2024 substrate with hotpress sintering technique. Different proportions of B_4C particles were used in AMMCs coating layer. The microstructural properties of the layer and substrate interface, microhardness, and adhesive wear resistance of the coating layer formed were examined. It was seen that Al and B_4C powders were homogeneously dispersed in the structure. According to microhardness results, it was determined that the hardness value on the coating layer enhanced with the increase of B_4C reinforcement particle volume rate. It is also found that with the increase of B_4C reinforcement particle ratio, wear resistance enhanced as well.

Acknowledgments

This study was funded by the Scientific Research Project Coordination Unit of Firat University Rectorate within the scope of Project No: TEKF. 19.08.

References

[1] M. Dilmec, M. Tinkir and H. Arikan, Investigation on influence of conditions of precipitation hardening process on the formability of AA2024 alloy, *Journal of the Fac. of Eng. and Arch.*, 30 (2015) 231-248.

[2] S. Buytoz, A. Orhan, A. K. Gur and U. Caligulu, Microstructural development of Fe-Cr-C and B_4C powder alloy coating on stainless steel by plasma-transferred arc weld surfacing, *Arab. J. Sci. Eng*,. 38 (2013) 2197-2204.

[3] F. Castillejo, J. Olaya and J. Alfonso, Wear and corrosion resistance of chromium-vanadium carbide coatings produced via thermo-reactive deposition, *Coatings,* 9 (2019) 1-13.

[4] J. Li, H. Cai, X. Xue and B. Jiang, The outward-inward growth behavior of microarc oxidation coatings in phosphate and silicate solution, *Mater. Lett*, 64 (2010) 2102-2104.

[5] L. Wen, Y. Wang, Y. Zhou, L. Guo and J. H. Ouyang, Microstructure and corrosion resistance of modified 2024 Al alloy using surface mechanical attrition treatment combined with microarc oxidation process, *Corros. Sci.*, 53 (2011) 473-480.

[6] H. Ni, J. Zhang, S. Lv, X. Wang, Y. Zhu and T. Gu, Preparation and performance optimization of original aluminum ash coating based on plasma spraying, *Coatings,* 9 (2019) 2-15.

[7] T. Laha, Y. Chen, D. Lahiri and A. Agarwal, Tensile properties of carbon nanotube reinforced aluminum nanocomposite fabricated by plasma spray forming, *Compos. Part A Appl. Sci. Manuf.,* 40 (2009) 589-594.

[8] M. Schem et al., CeO_2-filled sol-gel coatings for corrosion protection of AA2024-T3 aluminium alloy, *Corros. Sci.,* 51 (2009) 2304-2315.

[9] T. H. Hu, H. W. Shi, T. Wei, S. H. Fan, F. C. Liu and E. H. Han, Corrosion protection of AA2024-T3 by cerium malate and cerium malate-doped sol-gel coatings, *Acta Metall. Sin. (English Lett),* 32 (2019) 913-924.

[10] T. Guo, C. Kong, X. Li, P. Guo, Z. Wang and A. Wang, Microstructure and mechanical properties of Ti/Al co-doped DLC films: dependence on sputtering current, source gas, and substrate bias, *Appl. Surf. Sci.,* 410 (2017) 51-59.

[11] S. Zhou, L. Wang and Q. Xue, Controlling friction and wear of nc-WC/a-C(Al) nanocomposite coating by lubricant/additive synergies, *Surf. Coatings Technol.,* 206 (2012) 2698-2705.

[12] K. Feng et al., Improved high-temperature hardness and wear resistance of inconel 625 coatings fabricated by laser cladding, *J. Mater. Process. Technol.,* 243 (2017) 82-91.

[13] D. Zhang et al., Effect of in-situ synthesis of multilayer graphene on the microstructure and tribological performance of laser cladded Ni-based coatings, *Appl. Surf. Sci.,* 495 (2019) 143581.

[14] C. Shang et al., CoCrFeNi (W1 − xMox) high-entropy alloy coatings with excellent mechanical properties and corrosion resistance prepared by mechanical alloying and hot pressing sintering, *Mater. Des.,* 117 (2017) 193-202.

[15] W. Ge et al., Characterization and properties of CuZrAlTiNi high entropy alloy coating obtained by mechanical alloying and vacuum hot pressing sintering, *Adv. Powder Technol.,* 28 (2017) 2556-2563.

[16] C. Shang, E. Axinte, W. Ge, Z. Zhang and Y. Wang, High-entropy alloy coatings with excellent mechanical, corrosion resistance and magnetic properties prepared by mechanical alloying and hot pressing sintering, *Surfaces and Interfaces*, 9 (2017) 36-43.

[17] M. Yang, C. Xu, C. Wu, K. Lin, Y. J. Chao and L. An, Fabrication of AA6061/Al_2O_3 nano ceramic particle reinforced composite coating by using friction stir processing, *J. Mater. Sci.,* 45 (2010) 4431-4438.

[18] S. W. Cai, Y. Zong, T. S. Hua and R. G. Song, Study on the inhibition of hydrogen embrittlement of 7050 aluminum alloy in

humid air by MAO coating, *Anti-Corrosion Methods Mater.,* 67 (2020) 387-394.

[19] A. P. H. Mindivan, Wear and corrosion resistance of Ni-P coating on AA7075 aluminum alloy, *Mach. Technol. Mater.,* 31 (2016) 29-31.

[20] H. Asgharzadeh and M. Sedigh, Synthesis and mechanical properties of Al matrix composites reinforced with few-layer graphene and graphene oxide, *J. Alloys Compd.,* 728 (2017) 47-62.

[21] T. Yildiz, A. K. Gur and S. Aba, Examination of the wear behavior of Cu-Ni/B_4Cp composite by the Taguchi method, *Mater. Test.,* 56 (2014) 1009-1014.

[22] X. Li, Y. Gao, S. Wei and Q. Yang, Tribological behaviors of B_4C-hBN ceramic composites used as pins or discs coupled with B_4C ceramic under dry sliding condition, *Ceram. Int.,* 43 (2017) 1578-1583.

[23] L. Zhang et al., Microtopography and mechanical properties of vacuum hot pressing Al/B_4C composites, *Ceram. Int.,* 44 (2018) 3048-3055.

[24] Y. H. Celik and K. Secilmiş, Investigation of wear behaviours of Al matrix composites reinforced with different B_4C rate produced by powder metallurgy method, *Adv. Powder Technol.,* 28 (2017) 2218-2224.

[25] K. S. Kumar and V. S. Patnaik, Experimental investigation on aluminium alloy composites for wear behaviour, *International Conference on Electrical, Electronics, and Optimization Techniques (ICEEOT)* (2016) 3846-3852.

[26] G. H. Majzoobi and K. Rahmani, Mechanical characterization of Mg-B_4C nanocomposite fabricated at different strain rates, *Int. J. Miner. Metall. Mater.,* 27 (2020) 252-263.

[27] A. Singh et al., Effect reinforcement of boron carbide and silicon carbide on AA 2024 hardness, *Int. J. Sci. Res. Eng. Trends,* 5 (2019) 628-63.

[28] E. B. Moustafa and M. A. Taha, Evaluation of the microstructure, thermal and mechanical properties of Cu/SiC nanocomposites fabricated by mechanical alloying, *Int. J. Miner. Metall. Mater.,* 28 (2020) 475-486.

[29] I. Ovali, H. Karakoç and H. Çinici, Optimization of the wear resistance of AA2024 matrix composites fabricated with hot pressing, *J. Achiev. Mater. Manuf. Eng*., 79 (2016) 19-23.

[30] M. Rahimian, N. Parvin and N. Ehsani, The effect of production parameters on microstructure and wear resistance of powder metallurgy Al–Al_2O_3 composite, *Mater. Des.,* 32 (2011) 1031-1038.

[31] C. Saravanan, K. Subramanian, V. Anandakrishnan and S. Sathish, Tribological behavior of AA7075-TiC composites by powder metallurgy, *Ind. Lubr. Tribol.,* 70 (2018) 1066-1071.

[32] Z. C. Feng, Y. F. Liu, Y. Li, G. B. Sun, Z. Zhang and C. X. Shi, Microstructure and high temperature reciprocating sliding wear properties of $MoSi_2$/TiC/Γ-Ni composite coating in-situ synthesized by co-axial powder feeding plasma transferred arc cladding, *Tribol. Int.,* 129 (2018) 82-91.

[33] F. Toptan, A. Kilicarslan, A. Karaaslan, M. Cigdem and I. Kerti, Processing and microstructural characterisation of AA 1070 and AA 6063 matrix B_4Cp reinforced composites, *Mater. Des.,* 31 (2010) 87-91.

[34] P. Ashwath et al., Processing and characterization of extruded 2024 series of aluminum alloy, *Mater. Today Proc.,* 5 (2018) 12479-12483.

[35] P. Ashwath, J. Joel, M. A. Xavior and H. G. P. Kumar, Effect of SiC and Al_2O_3 particles addition to AA 2900 and AA 2024 MMC's synthesized through microwave sintering, *Mater. Today Proc.,* 5 (2018) 7329-7336.

[36] M. Ferry at al., Techno-economic study of aluminium alloy and steel as materials for deckhouses of offshore support vessels, *Indones. J. Nav. Archit.,* 1 (2013) 36-41.

[37] C.-J. Wang and S.-M. Chen, The high-temperature oxidation behavior of hot-dipping Al-Si coating on low carbon steel, *Surf. Coatings Technol.,* 200 (2006) 6601-6605.

[38] Z. Tang, F. Wang and W. Wu, Effect of a sputtered TiAlCr coating on the oxidation resistance of TiAl intermetallic compound, *Oxid. Met.,* 48 (1997) 511-525.

[39] G. Zhong-Xiang, W. Kai, Z. Yi-Sheng and Z. Bin, Cracking and interfacial debonding of the Al-Si coating in hot stamping of pre-coated boron steel, *Appl. Surf. Sci.,* 316 (2014) 595-603.

[40] I. Topcu, H. O. Gulsoy, N. Kadioglu and A. N. Gulluoglu, Processing and mechanical properties of B_4C reinforced Al matrix composites, *J. Alloys Compd.,* 482 (2009) 516-521.

[41] L. Zhang et al., Phase transformation and mechanical properties of B_4C/Al composites, *J. Mater. Res. Technol.,* 9 (2020) 2116-2126.

[42] M. Muratoğlu and M. Aksoy, The effects of temperature on wear behaviours of Al-Cu alloy and Al-Cu/SiC composite, *Mater. Sci. Eng. A,* 282 (2000) 91-99.

[43] D. Mummoorthi, M. Rajkumar and S. G. Kumar, Advancement and characterization of Al-Mg-Si alloy using reinforcing materials of Fe_2O_3 and B_4C composite produced by stir casting method, *J. Mech. Sci. Technol.,* 33 (2019) 3213-3222.

[44] P. Larsson, N. Axén and S. Hogmark, Tribofilm formation on boron carbide in sliding wear, *Wear,* 236 (1999) 73-80.

[45] K. M. Shorowordi, A. S. M. A. Haseeb and J. P. Celis, Tribo-surface characteristics of Al-B_4C and Al-SiC composites worn under different contact pressures, *Wear,* 261 (2006) 634-641.

[46] Y. H. Celik and E. Kilickap, Hardness and wear behaviours of al matrix composites and hybrid composites reinforced with B_4C and SiC, *Powder Metallurgy and Metal Ceramics,* 57 (2019) 613-622.

[47] H. Alrobei, Effect of different parameters and aging time on wear resistance and hardness of SiC-B_4C reinforced AA6061 alloy, *J. Mech. Sci. Technol.*, 34 (2020) 2027-2034.

[48] J. Zhou, J. Xu, S. Huang, Z. Hu, X. Meng and X. Feng, Effect of laser surface melting with alternating magnetic field on wear and corrosion resistance of magnesium alloy, *Surf. Coatings Technol.,* 309 (2017) 212-219.

[49] T. Courtney, *Mechanical Behavior of Materials*, McGraw Hill, Michigan (1990).

[50] J.-M. Wu, S.-J. Lin, J.-W. Yeh, S.-K. Chen, Y.-S. Huang and H.-C. Chen, Adhesive wear behavior of AlxCoCrCuFeNi high-entropy alloys as a function of aluminum content, *Wear,* 261 (2006) 513-519.

Cetin Ozay was born in 1978 in Maden-Elazig. He earned his B.Sc. from Firat University, Faculty of Tech. Education, Mechanical Edu. Dept., Elazig in 2000 and his M.Sc. and Ph.D. from Firat University, Institute of Science, Mechanical Dept., Elazig in 2004 and 2009, respectively. Since 2016, he has been working as an Associate Professor at the Firat University, Turkey. He is specialized in mechanical science, manufacturing, tribology, powder metallurgy, Taguchi, ANOVA.

Hasan Ballikaya was born in 1986 in Elazig. He received his B.Sc. from Firat University, Technical Education Faculty, Elazig in 2009. He also received M.Sc. in 2011 and Ph.D. in 2017 from Firat University, Institute of Science, Mechanical Dept., Elazig, respectively. Since 2018, he has been working as a Doctor at the University of Inonu, Turkey. He is specialized in mechanical science, manufacturing, ANSYS, CAD-CAM, Taguchi, ANOVA.

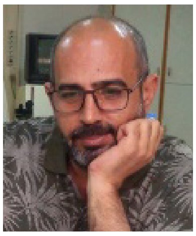

Fethi Dagdelen was born in 1975 in Palu-Elazig. He earned his B.Sc. from Fırat University, Faculty of Science, Department of Physics, Elazig in 1996. He also earned his M.Sc. and Ph.D. from Fırat University, Institute of Science, Physics Dept., Elazig in 1999 and in 2004, respectively. He has been working as an Associate Professor at the Firat University, Turkey since 2018. He investigates thermal properties and fabrication of the materials in material science.

Omer Etem Karlidag was born in 1990 in Elazig. He studied at Firat University, Faculty of Engineering, Mechanical Eng. Dept., Elazig in 2014. He received the M.Sc. from Firat University, Institute of Science and Technology, Mechanical Dept., Elazig, Turkey in 2017. He is specialized in manufacturing, powder metallurgy, and tribology.